Time-Resolved Observation of Excitation Hopping between Two Anthryl Moieties Attached to Both Ends of Alkanes: Simulation Based on Conformational Analysis

Tomiki Ikeda,*,† Bong Lee,† Shigeo Tazuke,†,‡ and Akio Takenaka§

Contribution from the Photochemical Process Division, Research Laboratory of Resources Utilization, and Department of Life Science, Faculty of Science, Tokyo Institute of Technology, 4259 Nagatsuta, Midori-ku, Yokohama 227, Japan. *Received November 10, 1989*

Abstract: Excitation hopping behavior in α,ω-bis(9-anthryl)-*n*-alkanes (An$(CH_2)_m$An (A*m*) with *m* = 3, 5, 7, 10, 12, 14, and 18) was explored by picosecond time-resolved fluorescence anisotropy measurements. The fluorescence anisotropy, $r(t)$, was found to decay with time for A7, A10, A12, A14, and A18, while in a model compound, 9-ethylanthracene (EA), $r(t)$ remained unchanged during its lifetime. Furthermore, no initial decay was observed for A3 and A5, though the residual polarization that is the $r(t)$ value at $t = \infty$ was clearly different from that of EA. This was interpreted in terms of extremely fast decay of $r(t)$ in A3 and A5, which was not detectable with our apparatus (10.73 ps/channel). In order to analyze the decay profiles of $r(t)$ of A*m*, conformational analysis was performed on the basis of potential energy calculations. The results were used to simulate the decay profiles of $r(t)$ on the basis of Förster's mechanism. The simulation demonstrated that the experimentally observed decay curves of $r(t)$ were well reproduced by the simulated curves, showing that excitation hopping in A*m* is satisfactorily analyzed by Förster's mechanism.

Nonradiative energy transfer in the molecular aggregate systems was first recognized by Gaviola et al.,[1] Weigert et al.,[2] and Levshin[3] in concentrated solutions of dye molecules. They noticed that emission from the concentrated dye solution was depolarized, whereas emission from the viscous dilute dye solution retained polarization. Since the discovery of the "concentrated depolarization phenomena", the energy migration process has been long realized as an important primary photophysical process in the molecular aggregate systems. For example, in polymers having identical chromophores along the polymer chains, excitation formed by absorption of photons at one chromophore site usually moves among the chromophores via the energy migration and is captured at a specific site called "trap", where subsequent processes like excimer formation take place.[4] Thus, if an acceptor molecule is incorporated in the polymer chain, the energy of photons may be collected with high efficiency at the site of the acceptor molecule. Taking advantage of this property, ideas of "antenna polymers"[5a,b] and "photon-harvesting polymers"[6] were proposed for the efficient collection of the energy of light, and many examples have been investigated.

However, it is very difficult to analyze strictly the excitation migration behavior in the molecular aggregate systems. Difficulties arise from the fact that in the molecular aggregate systems the location of the initially excited sites is not clearly defined. For example, in the polymers, the probability of excitation at the chain end is equal to that of the center of the polymer chain.[7] However, if the excitation migration operates, efficiency is definitely different between the two sites. Thus, for the analysis of the experimental results, account must be taken of distribution of the initially excited sites.[7] Another difficulty, much more serious for the exact analysis, is that excitation hops around in the system like a random walk; thus, following the locus of the excitation hopping is quite difficult even if we assume the dipole–dipole transfer a priori for the excitation hopping mechanism. If we assume that excitation hops in a polymer coil, we can draw many pathways for the excitation movements, between the nearest neighbors and between a pair that is far apart from each other along a polymer chain.[7] For such complicated systems, the exact solution of the problem becomes very difficult, requiring multiple averages over (1) initially excited sites, (2) local conformation, (3) distribution of acceptors, and so on, but approximation may be done. The most promising theoretical approach to this problem was developed by Fayer et al.,[8] Pearlstein et al.,[9] Haan and Zwanzig,[10] Blumen et al.,[11] Frank et al.,[12] and Whittington et al.[5c]

For analysis of the excitation migration behavior, *purely isolated bichromophoric systems* are superior to other molecular aggregate systems like polymers, since in the bichromophoric systems there are no complications associated with the distributions of the initially excited sites and the hopping pathway. A bichromophoric system with nonidentical donors and acceptors was already investigated in full detail by Stryer and Hangland[13] using oligomers of poly-L-proline, labeled at one end with a naphthyl (donor) and at the other end with a dansyl (acceptor) group. They used the sensitized fluorescence from the acceptor and obtained $R = 5.9 \pm 0.3$ dependence, which is in excellent agreement with Förster's theory. However, very few studies have been performed so far on the excitation migration in a bichromophoric system with *identical* chromophores.[14,15]

In the previous paper, we reported the excitation hopping behavior between two 2-naphthyl chromophores attached to both ends of alkanes by means of the picosecond time-resolved

* To whom correspondence should be addressed.
† Research Laboratory of Resource Utilization.
‡ Deceased, July 11, 1989.
§ Faculty of Science.

(1) Gaviola, E.; Pringsheim, P. *Z. Phys.* **1924**, *24*, 24.
(2) Weigert, F.; Kapper, G. *Z. Phys.* **1924**, *25*, 99.
(3) Levshin, W. L. *Z. Phys.* **1924**, *26*, 274.
(4) Soutar, I.; Phillips, D. In *Photophysical and Photochemical Tools in Polymer Science*; Winnik, M. A., Ed.; Reidel: Dordrecht, The Netherland, 1986; p 97.
(5) (a) Ren, X.-X.; Guillet, J. E. *Macromolecules* **1985**, *18*, 2012. (b) Guillet, J. E.; Rendall, W. A. *Ibid.* **1986**, *19*, 224. (c) Janse van rensburg, E. J.; Guillet, J. E.; Whittington, S. G. *Ibid.* **1989**, *22*, 4212.
(6) (a) Hargreaves, J. S.; Webber, S. E. *Macromolecules* **1985**, *18*, 734. (b) Bai, F.; Cheng, C.-H.; Webber, S. E. *Ibid.* **1986**, *19*, 2484.
(7) Frank, C. W.; Fredrickson, G. H.; Andersen, H. C. In *Photophysical and Photochemical Tools in Polymer Science*; Winnik, M. A., Ed.; Reidel: Dordrecth, The Netherlands, 1986; p 495.
(8) (a) Gochanour, C. G.; Andersen, H. C.; Fayer, M. D. *J. Chem. Phys.* **1979**, *70*, 4254. (b) Loring, R. F.; Andersen, H. C.; Fayer, M. D. *Ibid.* **1982**, *76*, 2015. (c) Ediger, M. D.; Fayer, M. D. *Ibid.* **1983**, *78*, 2518. (d) Peterson, K. A.; Fayer, M. D. *Ibid.* **1986**, *85*, 4702. (e) Baumann, J.; Fayer, M. D. *Ibid.* **1986**, *85*, 4087.
(9) (a) Perlstein, R. M. *J. Chem. Phys.* **1972**, *56*, 2431. (b) Hemenger, R. P.; Perlstein, R. M. *Ibid.* **1973**, *59*, 4064.
(10) Haan, S. W.; Zwanzig, R. *J. Chem. Phys.* **1978**, *68*, 1879.
(11) (a) Blumen, A.; Manz, J. *J. Chem. Phys.* **1979**, *71*, 4694. (b) Blumen, A.; Klafter, J.; Silbey, R. *Ibid.* **1980**, *72*, 5320.
(12) (a) Fredrickson, G. H.; Andersen, H. C.; Frank, C. W. *Macromolecules* **1983**, *16*, 1456. (b) Fredrickson, G. H.; Andersen, H. C.; Frank, C. W. *Ibid.* **1984**, *17*, 54. (c) Fredrickson, G. H.; Andersen, H. C.; Frank, C. W. *Ibid.* **1984**, *17*, 1496.
(13) Stryer, L.; Haughland, R. *Proc. Natl. Acad. Sci. U.S.A.* **1967**, *58*, 719.
(14) Moog, R. S.; Kuki, A.; Fayer, M. D.; Boxer, S. G. *Biochemistry* **1984**, *23*, 1564.
(15) Ikeda, T.; Lee, B.; Kurihara, S.; Tazuke, S.; Ito, S.; Yamamoto, M. *J. Am. Chem. Soc.* **1988**, *110*, 8299.

0002-7863/90/1512-4650$02.50/0

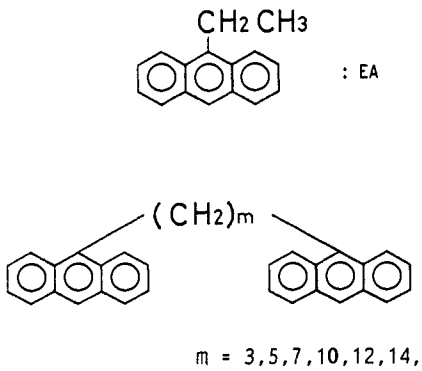

Figure 1. Structures of bichromophoric compounds used in this study.

fluorescence anisotropy measurements.[15] However, in that study, the poorly defined directions of the emission and the absorption transition dipoles of the 2-naphthyl chromophores led to "intrinsic averaging" over the orientation factor (κ^2) even in the absence of rotational diffusion of the chromophores; thus, strict evaluation of the time-resolved fluorescence anisotropy was impossible.[15]

In the present study, we evaluated the excitation hopping behavior between two 9-anthryl chromophores attached to both ends of alkanes, α,ω-bis(9-anthryl)-*n*-alkanes ($An(CH_2)_mAn$ (A*m*) with m = 3, 5, 7, 10, 12, 14, and 18), as well as in a model compound with a single chromophore, 9-ethylanthracene (EA), by means of the picosecond time-resolved fluorescence anisotropy measurements. The merit of the 9-anthryl chromophore is that it possesses clearly defined direction for the $S_0 \rightarrow S_1$ transition moment; thus, exact analysis based on Förster's equation is possible.

Although the bichromophoric compounds used in this study possess a great advantage in that analysis of the results of the time-resolved measurements is free from statistical considerations on the originally excited site and the hopping pathway, they have a disadvantage in that distribution must be taken into account for the interchromophore distance and the orientation of the two chromophores because of the flexible nature of the links between the two 9-anthryl chromophores. To overcome this problem, a conformational analysis of the bichromophoric compounds was performed. Calculation of potential energy of nonbonded atoms (van der Waals potential) in A*m* enabled us to estimate the distribution functions of the interchromophore distance and of the orientation of the two anthryl chromophores in the compounds. In A*m*, because of the definite direction of the transition moments, complete simulation of the time-resolved behavior of the fluorescence anisotropy could be performed with the aid of the results of the conformational analysis. In every conformation, the interchromophore distance, the orientation of the two relevant chromophores, and the orientation factor were calculated, and the hopping rate constant in that conformation was calculated by applying Förster's equation. On the assumption that the distribution of the conformations obeys the Boltzmann distribution, we performed the computer simulation of the expected decays of the fluorescence anisotropy. Comparison of the experimentally observed fluorescence anisotropy decays with those obtained by the simulation procedure revealed that the computer simulation accounts well for the observed decays.

Experimental Section

Materials. Structures of the bichromophoric compounds and the model compound used in this study are shown in Figure 1.

9-Ethylanthracene (EA). To the Grignard reagent prepared from Mg (2 g) and bromoethane (6 mL) in anhydrous ethyl ether (60 mL) was added a hot solution of anthrone (8 g) in anhydrous benzene (50 mL). The reaction mixture was stirred and refluxed under nitrogen for 2 h, until the mixture became green. After the solution was cooled and decomposed with ice and 6 N hydrochloric acid, the solvents were evaporated and the residue was washed 10 times with hot 10% NaOH solution to remove unreacted anthrone. The crude product was washed with water, dried, and chromatographed on a silica gel column with dichloromethane–*n*-hexane (1:4) as eluent. The colorless prisms of EA were obtained by recrystallization from ethanol: mp 55–57 °C; IR (KBr) 3050, 2930, 2850, 1620, 1450, 1310 cm^{-1}; ^1H NMR (CD_2Cl_2) δ 1.5 (t, 3, J = 7.5 Hz), 3.6 (q, 2, J = 12 Hz), 7.4–8.4 (m, 9). Anal. Calcd for $C_{16}H_{14}$: C, 93.20; H, 6.80. Found: C, 93.11; H, 6.83.

1,3-Bis(9-anthryl)propane (A3). The anhydrous ethyl ether solution of 1,3-dibromopropane (2.11 mL) was added dropwise to the stirred Mg (1.46 g) dispersion in anhydrous ethyl ether. After the mixture was refluxed for 1 h, the anhydrous benzene solution (50 mL) of anthrone (9 g) was added dropwise. The reaction mixture was stirred and refluxed under nitrogen for 10 h. After the mixture was cooled in an ice bath, 6 N hydrochloric acid (60 mL) was added and the solvents were evaporated to dryness. The residue was washed 10 times with hot 10% NaOH solution and with water, dried, and chromatographed on a silica gel column with dichloromethane–*n*-hexane (1:4) as eluent. The light yellow crystalline A3 was obtained by recrystallization from ethanol: mp 197–200 °C; IR (KBr) 3050, 2930, 2850, 1620, 1450, 1310 cm^{-1}; ^1H NMR (CD_2Cl_2) δ 1.1–1.5 (m, 1), 3.5 (t, 2, J = 7.5 Hz), 7.4–8.5 (m, 9). Anal. Calcd for $C_{31}H_{24}$: C, 93.94; H, 6.06. Found: C, 93.57; H, 5.84.

1,5-Bis(9-anthryl)pentane (A5). The mixture of 9-anthraldehyde (2.06 g) and acetone (0.37 mL) in ethanol (30 mL) was added to the ethanol solution of NaOH (3 g). After the mixture was stirred at room temperature for 1 h, the insoluble yellow product formed was filtered, washed with water, and recrystallized from benzene–chloroform, giving yellow crystalline 1,5-bis(9-anthryl)-1,4-pentadien-3-one. The ethylenic part of this ketone was reduced by refluxing with zinc dust (25 g) in acetic acid (150 mL). The reaction mixture was refluxed for an additional 2 h, and then it was poured into water and extracted with dichloromethane. The product was recrystallized from carbon tetrachloride.

The ketone (2.65 g) was reduced by refluxing for 2 h in triethylene glycol (20 mL) containing hydrazine (2 mL, 80%) and NaOH (0.9 g). The mixture was diluted with water and extracted with benzene. The product was chromatographed on a silica gel column with dichloromethane–*n*-hexane (1:4) as eluent. Pure A5 was obtained by recrystallization from ethanol: mp 173–175 °C; IR (KBr) 3040, 2920, 2850, 1610, 1460, 1300 cm^{-1}; ^1H NMR (CD_2Cl_2) δ 1.7–2.0 (m, 3), 3.6 (t, 2, J = 7.5 Hz), 7.4–8.5 (m, 9). Anal. Calcd for $C_{33}H_{28}$: C, 93.40; H, 6.60. Found: C, 93.95; H, 6.53.

1,7-Bis(9-anthryl)heptane (A7), 1,10-bis(9-anthryl)decane (A10), 1,12-bis(9-anthryl)dodecane (A12), 1,14-bis(9-anthryl)tetradecane (A14), and 1,18-bis(9-anthryl)octadecane (A18) were prepared by the same method as that for A3. 1,7-Dibromoheptane, 1,10-dibromodecane, 1,12-dibromododecane, 1,14-dibromotetradecane, and 1,18-dibromooctadecane were used instead of 1,3-dibromopropane for A7, A10, A12, A14, and A18, respectively. Analytical results are shown below.

A7: mp 120–122 °C; IR (KBr) 3030, 2920, 2840, 1620, 1460, 1310 cm^{-1}; ^1H NMR (CD_2Cl_2) δ 1.4–1.9 (m, 5), 3.5 (t, 2, J = 7.5 Hz), 7.4–8.5 (m, 9). Anal. Calcd for $C_{35}H_{32}$: C, 92.92; H, 7.08. Found: C, 92.64; H, 7.24.

A10: mp 155–157 °C; IR (KBr) 3030, 2930, 2840, 1610, 1450, 1310 cm^{-1}. ^1H NMR (CD_2Cl_2) δ 1.1–2.1 (m, 8), 3.6 (t, 2, J = 7.5 Hz), 7.4–8.5 (m, 9). Anal. Calcd for $C_{38}H_{38}$: C, 92.31; H, 7.69. Found: C, 92.54; H, 7.97.

A12: mp 104–107 °C; IR (KBr) 3040, 2930, 2850, 1620, 1450, 1310 cm^{-1}; ^1H NMR (CD_2Cl_2) δ 1.1–2.3 (m, 10), 3.5 (t, 2, J = 7.5 Hz), 7.4–8.6 (m, 9). Anal. Calcd for $C_{40}H_{42}$: C, 91.95; H, 8.05. Found: C, 91.23; H, 8.11.

A14: mp 63–66 °C; IR (KBr) 3040, 2930, 2850, 1620, 1450, 1310 cm^{-1}; ^1H NMR (CD_2Cl_2) δ 1.1–2.6 (m, 12), 3.5 (t, 2, J = 7.5 Hz), 7.4–8.5 (m, 9). Anal. Calcd for $C_{42}H_{46}$: C, 91.64; H, 8.36. Found: C, 91.05; H, 8.68.

A18: mp 76–79 °C; IR (KBr) 3050, 2930, 2850, 1620, 1450, 1310 cm^{-1}; ^1H NMR (CD_2Cl_2) δ 1.2–2.8 (m, 16), 3.5 (t, 2, J = 7.5 Hz), 7.4–8.5 (m, 9). Anal. Calcd for $C_{46}H_{54}$: C, 91.09; H, 8.91. Found: C, 90.83; H, 9.32.

2-Methyltetrahydrofuran (MTHF) was used in the spectroscopic measurements throughout this work. MTHF (Tokyo Kasei) was washed with 10% NaOH, dried over $MgSO_4$ and then CaH_2, and finally distilled fractionally over sodium metal twice.

All samples were thoroughly degassed by several freeze–pump–thaw cycles under high vacuum ($\sim 10^{-5}$ mmHg) and then sealed off for the spectroscopic measurements.

Measurements. Absorption spectra were recorded on a Hitachi UV-320 spectrophotometer, and corrected fluorescence and excitation spectra were measured on a Hitachi F-4000 fluorescence spectrometer.

In order to exclude the contribution of rotational diffusion of the chromophores to the fluorescence depolarization, both the steady-state and time-resolved fluorescence anisotropy measurements were performed at 77 K in glass matrix of MTHF at 10^{-5}–10^{-6} M.

A time-correlated single-photon counting method was used to measure the fluorescence and the fluorescence anisotropy decays. Since detailed

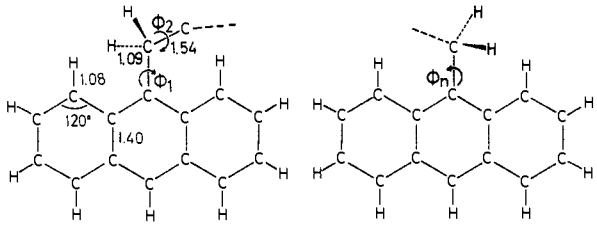

Figure 2. Structural parameters of A*m* used for the conformational analysis.

description of the system has been given already,[15] we briefly outline the system here. A synchronously pumped, cavity-dumped dye laser (Spectra Physics 375B and 344S) operated with a mode-locked Nd:YAG laser (Spectra Physics 3460 and 3240) was an excitation pulse source with a pulse width of 6 ps (full width at half-maximum, fwhm). For excitation of samples, frequency doubling was achieved with a KDP crystal (Inrad 531). Fluorescence was monitored at right angles to the excitation path through a monochromator (Jasco CT-25C) with a microchannel plate photomultiplier (Hamamatsu R1564U-01). Signals from the photomultiplier were amplified with a 1.3-GHz preamplifier (HP 8447D), discriminated with a constant-fraction discriminator (Ortec 583), and used as a stop pulse for a time to amplitude converter (TAC; Ortec 457). A start pulse was provided from a fast photodiode (Antel AR-S2) monitoring a laser pulse through a discriminator (Ortec 436). Data from the TAC were stored in a multichannel analyzer (Canberra 35 Plus) and then transferred to a microcomputer (NEC PC9801) where decay analysis was performed by an iterative nonlinear least-squares method.

Time-resolved decays of the fluorescence anisotropy were measured with pulsed excitation. A vertically polarized excitation light pulse was obtained through a Babine–Soleil compensator, and $I_{\parallel}(t)$ and $I_{\perp}(t)$ were measured alternatively through a polarizer, which was placed in front of the monochromator. Here, $I_{\parallel}(t)$ and $I_{\perp}(t)$ represent the fluorescence intensities observed with parallel and perpendicular orientations of the polarizer to the excitation pulse. $I_{\parallel}(t)$ and $I_{\perp}(t)$ were measured alternatively by rotating the polarizer periodically in order to eliminate any artifacts due to the long-term laser instability. A depolarizer was also placed just before the monochromator to remove anisotropic characteristics of the monochromator against $I_{\parallel}(t)$ and $I_{\perp}(t)$.

The fluorescence anisotropy, $r(t)$, was calculated by eq 1 where deconvolution of the instrument response function was performed.

$$r(t) = [I_{\parallel}(t) - I_{\perp}(t)]/[I_{\parallel}(t) + 2I_{\perp}(t)] \quad (1)$$

In every run, more than 50000 counts were accumulated at the maximum channel to ensure reliable values of $r(t)$.

Conformational Analysis. Conformational analysis was performed on the basis of potential energy calculations including the van der Waals interaction between nonbonded atoms and the intrinsic torsional potential energies associated with rotation about C–C bonds.[15-18] For calculation of the van der Waals interaction, Lennard-Jones potential function was employed in which the potential energy V_{ij} between the ith and jth nonbonded atoms is expressed by eq 2 where d_{ij} is the distance between the ith and jth nonbonded atoms and A_{ij} and B_{ij} are coefficients.

$$V_{ij} = B_{ij}/d_{ij}^{12} - A_{ij}/d_{ij}^{6} \quad (2)$$

The attractive term coefficient A_{ij} in eq 2 can be determined by applying the Slater–Kirkwood equation modified by Scott and Scheraga,[19] but in this study we adopted the A_{ij} and B_{ij} values reported in the literature.[17] The potential function was modified by considering the molecule–solvent interaction according to the procedure employed by Flory.[20] Calculations was performed by the use of the potential functions given in eq 3 where V_{ij}^0 is the value of V_{ij} at $d_{ij} = d_{ij}^0$ (the sum of the van der Waals radii of the interacting atom).

$$V_{ij}^* = V_{ij} - V_{ij}^0 \qquad d_{ij} < d_{ij}^0$$
$$V_{ij}^* = 0 \qquad d_{ij} \geq d_{ij}^0 \quad (3)$$

The total potential energy due to the van der Waals interaction was calculated as the sum over all pairs of nonbonded atoms. The intrinsic torsional potential energy for the skeletal alkyl chain, $E_{tor}(\phi)$, was calculated for the rotational angle ϕ by eq 4 where E_0 is the torsional barrier energy (E_0 = 2.8 kcal/mol).[21]

$$E_{tor}(\phi) = (E_0/2)(1 + \cos(3\phi)) \quad (4)$$

The total potential energy was obtained as the sum of the potential energies due to the van der Waals interaction and the intrinsic torsional potentials.

Structural parameters used in this calculation are shown in Figure 2. The parameters for the anthryl moieties were obtained from X-ray data of the anthracene crystal,[22] and the parameters of the skeletal alkane chain were those used by Abe et al.[21] For the calculation of the potential energies of A*m*, $m + 1$ rotational angles, $\phi_1, \phi_2, \ldots, \phi_{m+1}$, were taken into account (Figure 2).

The fraction of the ith conformation, f_i, was calculated by eq 5 on the assumption that the distribution of conformations obeys the Boltzmann distribution where E_i is the calculated potential energy for the ith conformation.

$$f_i = \exp(-E_i/RT)/\sum \exp(-E_i/RT) \quad (5)$$

On every conformation, the interchromophore distance (R) and the angles between two vectors along the long axis of the chromophore rings (θ_L) and along the short axis of the chromophore rings (θ_S) were calculated, and the distribution functions for R, θ_L, and θ_S were evaluated on the basis of eq 5. Here, R was defined as the distance between the centers of the two anthracene rings.

Table I. Fluorescence Quantum Yields of A*m* and EA[a]

	ϕ_F (RT)		ϕ_F (77 K)
	MTHF	MCH[b]	MTHF
EA	0.33	0.32	0.51
A3	0.47	0.47	0.52
A5	0.46	0.47	0.52
A7	0.45	0.41	0.53
A10	0.45	0.47	0.51
A12	0.42		0.53
A14	0.37		0.51
A18	0.34		0.51

[a] Determined by taking quinine sulfate as the standard. [b] Data from ref 23; measured in methylcyclohexane (MCH).

Table II. Analysis of Fluorescence Decay Profiles of A*m* and EA[a]

	A	τ, ns	χ^2	DW
EA	1.325	11.8	1.0912	1.9179
A3	1.299	9.1	1.1273	1.8516
A5	1.185	10.7	1.0454	1.8383
A7	1.134	11.5	1.0833	1.6995
A10	1.584	11.3	1.1875	1.7339
A12	1.240	11.2	1.1184	1.7675
A14	1.026	10.6	1.2531	1.7879
A18	1.586	11.0	1.1361	1.6457

[a] λ_{ex} = 347 nm, λ_{em} = 393 nm; measured in MTHF at 77 K; analysis based on $I(t) = A \exp(-t/\tau)$.

Results

Absorption and Fluorescence Spectra and Fluorescence Lifetimes. At room temperature, A5 and A14 showed clear excimer emission in MTHF, while other bichromophoric molecules, A7, A10, and A12, showed negligibly weak excimer emission. Of note is the absence of excimer fluorescence in the spectrum of A3, which is in contrast to the behavior of other bis(aryl)propanes such as 1,3-bis(2-naphthyl)propane.[15] This may be due to extremely high rate of photocyclization in the singlet excited state of A3.[23] Thus, when face-to-face conformation of the two anthryl moieties in A3 is achieved, the photodimerization will take place immediately.

In a rigid glass matrix of MTHF at 77 K, no excimer emission was observed in all the bichromophoric molecules. Furthermore, no photoreaction seemed to proceed to any appreciable extent even in A3. This was confirmed by monitoring the fluorescence in-

(16) Flory, P. J. *Statistical Mechanics of Chain Molecules*; Wiley: New York, 1969.
(17) Hopfinger, A. J. *Conformational Properties of Macromolecules*; Academic: New York, 1973.
(18) Ito, S.; Yamamoto, M.; Nishijima, Y. *Bull. Chem. Soc. Jpn.* **1982**, *55*, 363.
(19) Scott, R. A.; Scheraga, H. A. *J. Chem. Phys.* **1965**, *42*, 2209.
(20) Brant, D. A.; Flory, P. J. *J. Am. Chem. Soc.* **1965**, *87*, 2791.
(21) Abe, A.; Jernigan, R. L.; Flory, P. J. *J. Am. Chem. Soc.* **1966**, *88*, 631.
(22) Cox, P. J.; Sim, G. A. *Acta. Crystallogr. Sec. B* **1979**, *35*, 404.
(23) Castellan, A.; Desvergne, J.-P.; Bouas-Laurent, H. *Chem. Phys. Lett.* **1980**, *76*, 390.

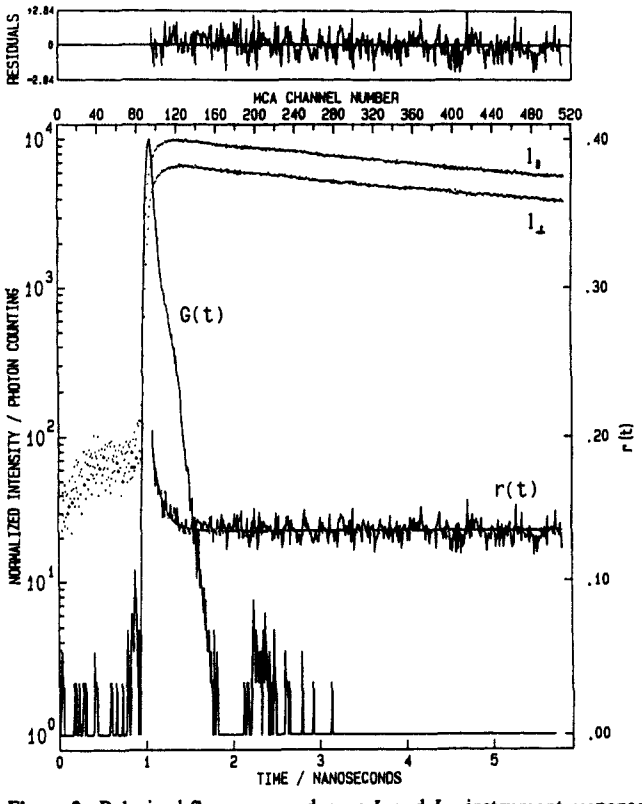

Figure 3. Polarized fluorescence decays $I_\parallel$ and $I_\perp$, instrument response function $G(t)$, and anisotropy decay $r(t)$ of A12 in MTHF at 77 K: λ_{ex} = 370 nm, λ_{em} = 417 nm; time division, 11.36 ps/channel. The solid line shows the best fit curve based on eq 14 (see Table III and Discussion).

tensity of A*m* under photoirradiation of the ^1L_a band of the anthryl compounds. At 77 K, all the compounds, A*m* and EA, showed nearly identical fluorescence and absorption spectra except A3 in which both spectra were red-shifted by ~3 nm in comparison with those of the other compounds.

In Table I are listed the values of the fluorescence quantum yield (ϕ_F), which include both the locally excited and excimer emissions. At room temperature, ϕ_F of EA is lower than those of A*m*; however, we can recognize a clear tendency that by increasing the alkyl spacer length (m), the ϕ_F value approaches that of EA. On the other hand, at 77 K the ϕ_F values are nearly identical in all compounds.

In Table II are shown the results of the fluorescence lifetime analysis of A*m* and EA. Measurements were performed at 77 K in the glass matrix with λ_{ex} = 347 nm and λ_{em} = 393 nm. In principle, the fluorescence decay curves were satisfactorily analyzed by a single-exponential function with the lifetime of ~11 ns as judged by reduced χ^2 and Durbin–Watson (DW) parameters. However, the lifetime of A3 was somewhat shorter than those of the other molecules, although the single-exponential function was still satisfactory enough to describe the decay profile. This may be another indication of some weak interaction between two anthryl moieties in A3, leading to the quenching of the singlet excited state.

Fluorescence Anisotropy Decays. In Figure 3 are shown $I_\parallel$ and $I_\perp$, instrument response function $G(t)$, and anisotropy decay $r(t)$, of A12 measured in MTHF at 77 K. Figure 4 shows the anisotropy decays of all compounds. It is clearly seen that $r(t)$ for EA does not change with time, which indicates that excitation remains at the originally excited site during its lifetime. In A*m* with $m \geq 7$, the decay of $r(t)$ is clearly observed. This means that emission from a transition moment, which is different from that of the originally excited site, contributes to the observed emission and is a clear piece of evidence that excitation hopping takes place between the two 9-anthryl moieties attached to both ends of alkanes. In A3 and A5, no decay of $r(t)$ was observed even in the shortest time range available (10.73 ps/channel) for our time-resolved measurement system. However, in both compounds, residual polarization r_∞, which is the $r(t)$ value at $t = \infty$, is different from the $r(t)$ value observed in EA; thus, it is reasonably assumed that in these compounds the decay of $r(t)$ is too fast to be detectable with our apparatus.

Conformational Analysis. The conformational energy map for A3 is shown in Figure 5 as a function of ϕ_2 and ϕ_3, where ϕ_1 and ϕ_4 were fixed at 90°. This energy map was constructed from the results of the potential energy calculation at intervals of 5° for ϕ_2 and ϕ_3. Contours are drawn at intervals of 0.5 kcal/mol relative to the energy minima. Figure 5 demonstrates that the most stable conformation is situated at tt ($\phi_2 = \phi_3 \sim 180°$) and is surrounded by four equivalent tg conformations. It is of particular interest to compare the stable conformations of 1,3-bis(2-naphthyl)propane (N3), which was studied in detail in our previous publication,[15] with those of A3. In the former, the gg conformations ($\phi_2 = \phi_3 \sim 60°$ and $\phi_2 = \phi_3 \sim 300°$) were also involved in the stable conformations, while in A3 such conformations are excluded from

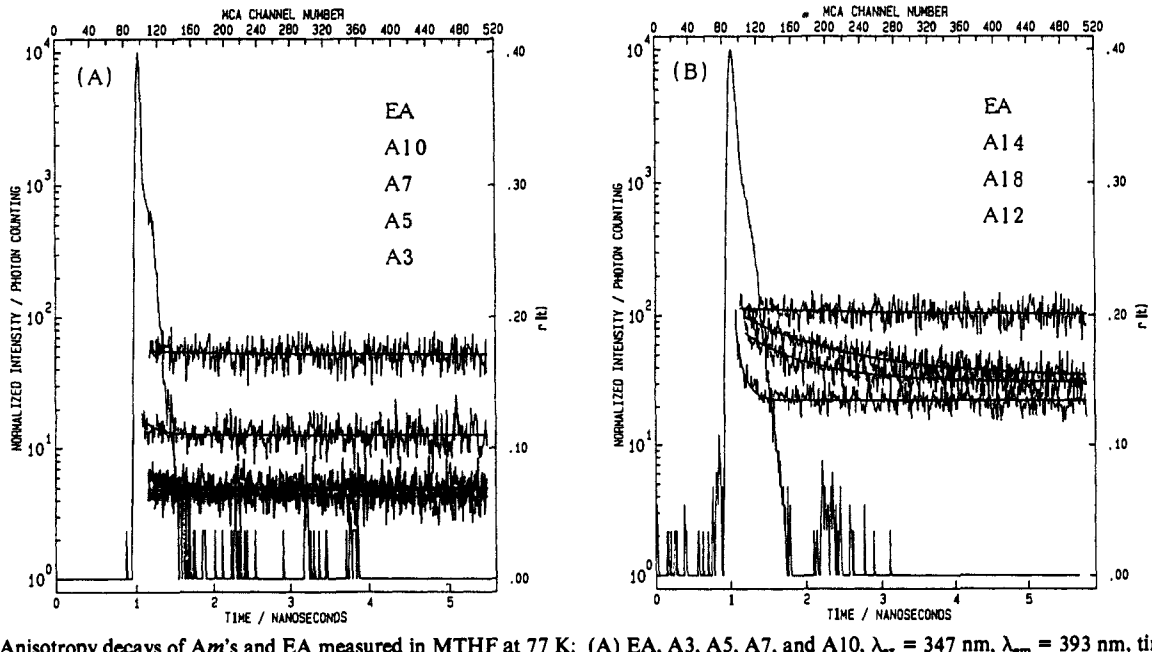

Figure 4. Anisotropy decays of A*m*'s and EA measured in MTHF at 77 K: (A) EA, A3, A5, A7, and A10, λ_{ex} = 347 nm, λ_{em} = 393 nm, time division 10.73 ps/channel. (B) EA, A12, A14, A18, λ_{ex} = 370 nm, λ_{em} = 417 nm, time division 11.36 ps/channel. The solid lines show the best fit curves based on eq 14 (see Table III and Discussion).

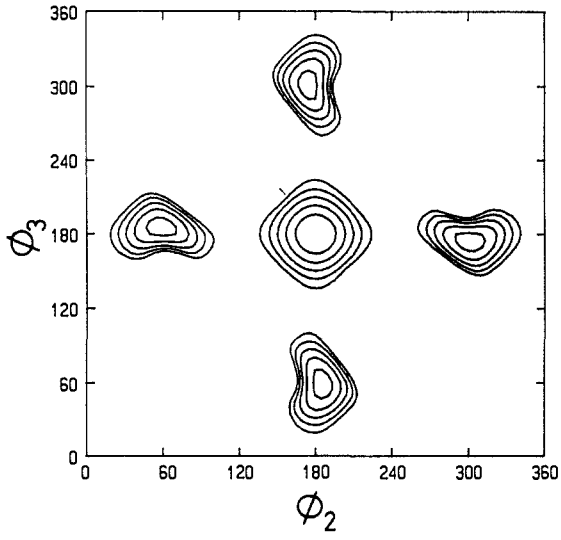

Figure 5. Conformational energy map for A3 as a function of ϕ_2 and ϕ_3. ϕ_1 and ϕ_4 were fixed at 90°. Contours are shown at intervals of 0.5 kcal/mol relative to the energy minima.

the stable conformation. This result clearly indicates that the 9-anthryl moiety is much more bulky than the 2-naphthyl group; thus, the number of the stable conformations is limited in A*m* compounds.

Potential energy calculations on A5, A7, A10, and A12 were carried out in the same way as for A3. However, the interval of calculation for A5 and A*m* ($m \geq 7$) was 60° and 120, respectively. The models considered for A*m* with $m \geq 7$ are the rotational isomeric state model where all C–C bonds of the methylene chain are assumed to be one of three rotational isomers: trans, gauche(+), and gauche(−). The feasibility of this model for rather short polymethylene chains like those considered here was discussed already.[15]

The conformational energy maps for A3 as a function of ϕ_3 and ϕ_4 are shown in Figure 6, where ϕ_1 and ϕ_2 were fixed at 90° and 180° (a) and at 90° and 60° (b), respectively, and calculation was performed at 5° intervals. Figures 6 shows a remarkable feature of 9-anthrylalkanes that the stable conformation is limited only in the small range of the rotational angles of ϕ_3 and ϕ_4 due to the steric hinderance of the bulky 9-anthryl moieties. This is in sharp contrast to the conformation of 2-naphthylalkanes in which the potential energies are insensitive to the rotation of the naphthalene ring.[15]

Distribution functions of interchromophore distance (R) for A*m* at 77 K are shown in Figure 7, where calculation of the distribution was performed at an increment of 0.2. It is clearly seen that in A3 the distribution of R is quite narrow at 77 K and bimodal with two maxima at R = 6.4 and 7.6. The fraction of the stable conformer with R = 7.6, which corresponds to a conformation with the all-trans configuration in the skeleton chain ($\phi_2 - \phi_3 = 180°$) is more than 0.6. In A*m* with $m \geq 5$, the distribution is broader as expected from the increased number of skeletal atoms. An ensemble-averaged interchromophore distance, $\langle R \rangle$, was calculated by eq 6 where R_i is the interchromophore distance of the ith conformer and $f_i(R_i)$ is the fraction of the ith conformers. The $\langle R \rangle$ values thus calculated are 7.05 (A3), 9.45 (A5), 11.28 (A7), 13.84 (A10), and 15.45 Å (A12).

$$\langle R \rangle = \sum R_i f_i(R_i) / \sum f_i(R_i) \qquad (6)$$

Angular distributions of θ_L and θ_S in A*m* at 77 K are shown in Figures 8 and 9, respectively. These angular distribution functions were computed with fixed rotational angles of $\phi_1 = \phi_{m+1} = 90°$.

Simulation of Fluorescence Anisotropy Decay Curves. Simulation of the fluorescence anisotropy decay curves was performed on the basis of the conformational analysis. As described in the Experimental Section, on each conformation, the interchromophore distance (R_i), the angle between two vectors along the long axis

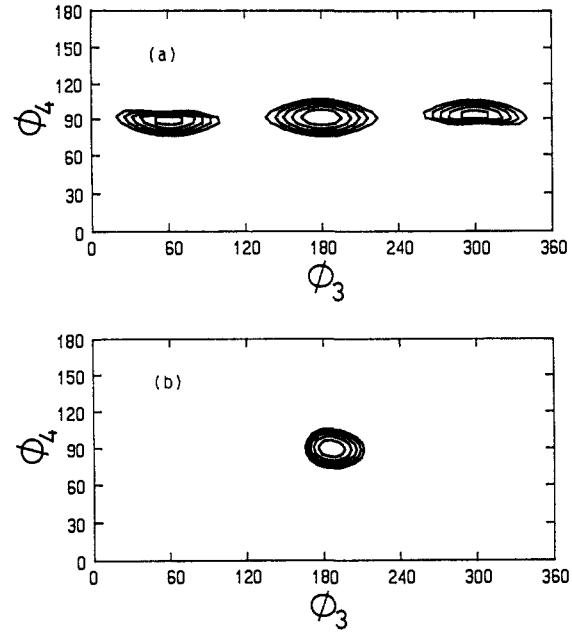

Figure 6. Conformational energy map for A3 as a function of ϕ_3 and ϕ_4. ϕ_1 and ϕ_2 were fixed at 90° and 180° (a) and at 90° and 60° (b), respectively. Contours are shown at intervals of 0.5 kcal/mol relative to the energy minima.

(θ_{Li}) and the short axis (θ_{Si}) of the anthracene ring, and the orientation factor defined by eq 7 were calculated.[24]

$$\kappa_i = \cos \theta_{DAi} - 3 \cos \theta_{Di} \cos \theta_{Ai} \qquad (7)$$

Here, θ_{DAi} is the angle between the transition moment vectors of the donor and the acceptor and θ_{Di} and θ_{Ai} are the angles between these transition moments and the direction of R_i, respectively. It is well-known that the ^1L_a band in the anthracene derivatives corresponds to the $S_0 \rightarrow S_1$ transition, and its transition moment lies along the short axis of the anthracene ring.[25] Thus, in A*m* and EA, θ_{DAi} in eq 7 can be reasonably replaced by θ_{Si}.

In the incoherent excitation hopping between two identical chromophores, the following equation is applicable to describe the fluorescence anisotropy decay profiles:[14,15]

$$r(t) = \tfrac{1}{2}(r_0 - r_1) \exp(-2\omega t) + \tfrac{1}{2}(r_0 + r_1) \qquad (8)$$

Here, r_0 is the limiting value of r and can be estimated from a case where no fluorescence depolarization occurs. Thus, the r_0 value for the present case can be determined from the r_0 value of EA. r_1 is the anisotropy of fluorescence emitted entirely by the chromophore that is not originally excited. In the simulation procedure, we calculated the r_1 value of the ith conformer (r_{1i}) by eq 9.[24] In eq 8, ω is the hopping rate constant. If we assume

$$r_{1i} = (r_0/2)(3 \cos^2 \theta_{Si} - 1) \qquad (9)$$

Förster's mechanism for the excitation migration, ω of the ith conformer with R_i and κ_i can be written in the form of eq 10.[24]

$$\omega_i = \frac{9(\ln 10)\phi_D}{128\pi^5 N n^4 \tau_D} \frac{\kappa_i^2}{R_i^6} J(\nu) \qquad (10)$$

Here, N is Avogadro's number, ϕ_D and τ_D are the donor emission quantum yield and lifetime in the absence of the acceptor, $J(\nu)$ is the spectral overlap intergral of the donor emission and the acceptor absorption, and n is the refractive index of the medium. With respect to ϕ_D and τ_D, we can use the values of ϕ_F and τ of EA (Tables I and II). $J(\nu)$ was determined from the absorption and the fluorescence spectra of EA as 1.5×10^{15} cm^6/mol at 77

(24) Dale, R.; Eisinger, J. In *Biochemical Fluorescence: Concept*; Chen, R. F., Edelhoch, H., Ed.; Marcel Dekker: New York, 1975; Vol. 1, p 115.
(25) Birks, J. B. *Photophysics of Aromatic Molecules*; Wiley: New York, 1970.

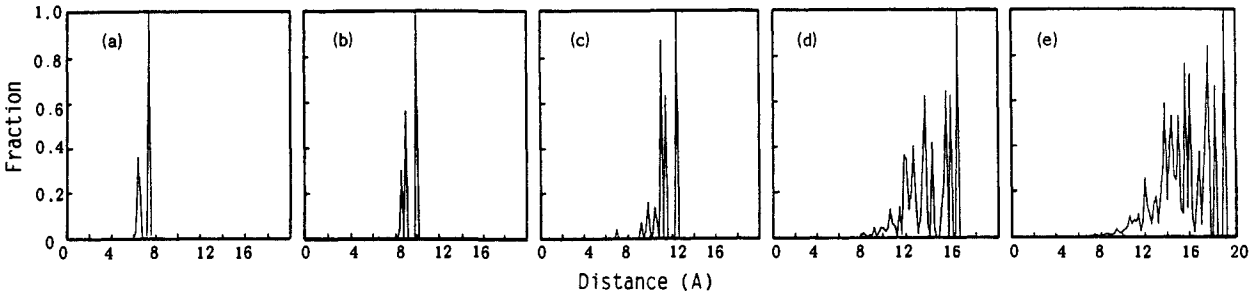

Figure 7. Distribution functions of interchromorphore distance for (a) A3, (b) A5, (c) A7, (d) A10, and (e) A12 at 77 K.

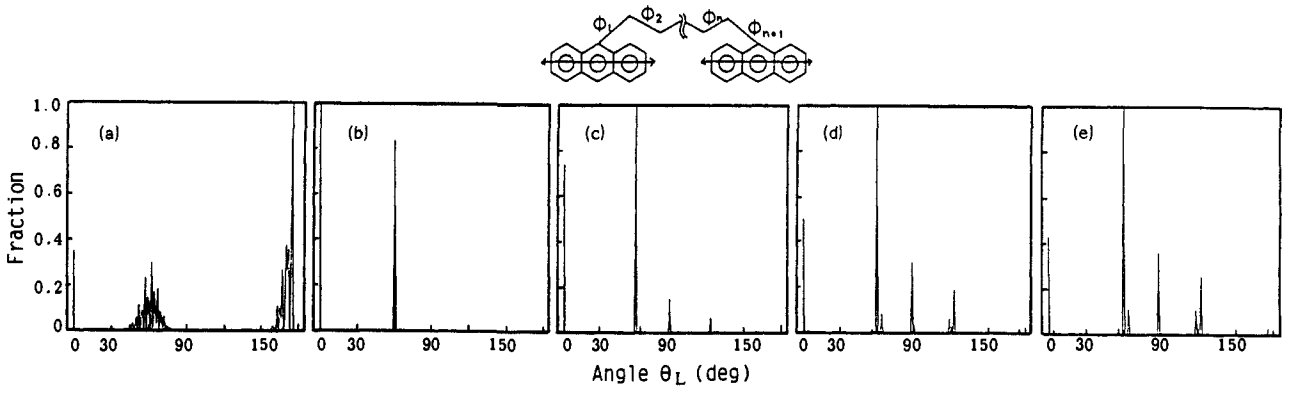

Figure 8. Angular distributions of the two vectors along the long axis (θ_L) of the anthracene ring. Key: (a) A3; (b) A5; (c) A7; (d) A10; (e) A12.

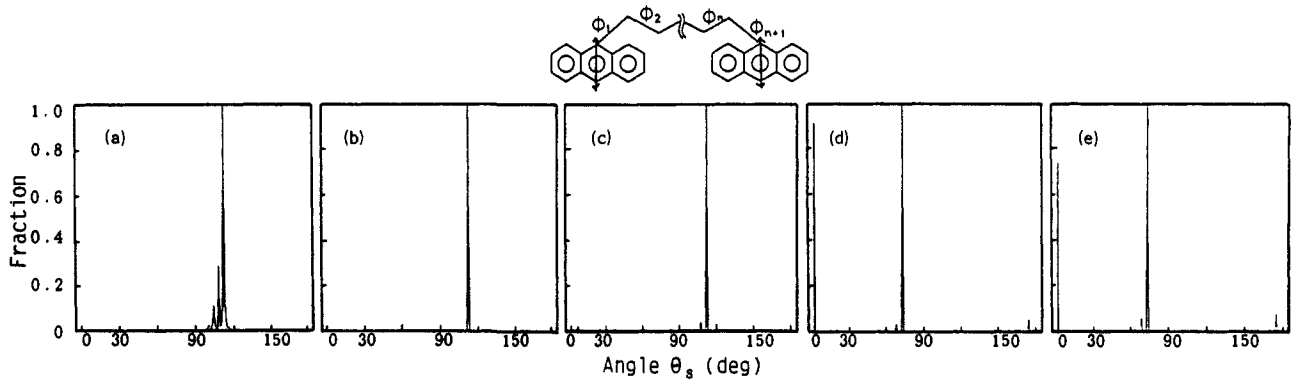

Figure 9. Angular distributions of the two vectors along the short axis (θ_S) of the anthracene ring. Key: (a) A3; (b) A5; (c) A7; (d) A10; (e) A12.

K. This value is somewhat larger than the value reported for 9-methylanthracene at room temperature.[26] With respect to n of MTHF at 77 K, it has not been reported so far; thus, we used a value at 20 °C (1.405).[27] Substituting these values in eq 10, we obtain a simpler expression for ω_i

$$\omega_i = \frac{K\kappa_i^2}{R_i^6} \tag{11}$$

where

$$K = \frac{9(\ln 10)\phi_D}{128\pi^5 N n^4 \tau_D} J(\nu) \tag{12}$$

By substituting eqs 9 and 11 in eq 8, we obtain the expected decay of the fluorescence anisotropy, $r_i(t)$, for one particular conformation i. The observable decay of the fluorescence anisotropy can be obtained by ensemble-averaging over all conformations on the assumption that the distribution of the conformations obey the Boltzmann distribution.

$$r(t) = \sum r_i(t) \exp(-E_i/RT) / \sum \exp(-E_i/RT)$$
$$= \sum r_i(t) f_i \tag{13}$$

Our program of the fluorescence anisotropy simulation enabled us to draw the expected decay profiles in any time region. Figure 10 shows the expected decays of $r(t)$ in three time regions. In Figure 10a, the time division is 0.1 ps/channel, which is not obtainable in our apparatus, and parts b and c of Figure 10 show the results of the simulation with the same time division (10.73 and 11.36 ps/channel) as employed in our time-resolved anisotropy measurements (Figures 3 and 4).

Discussion

In the present study, we performed the computer simulation of the decay profiles of the fluorescence anisotropy $r(t)$ by appling strictly Förster's equation to the results obtained by the conformational analysis. In our simulation procedure, no variables (fitting parameters) are involved. Only experimentally determined parameters are used: ϕ_D, τ_D, and $J(\nu)$, which can be unequivocally determined from the model compound EA. Simulation on the basis of the strict application of Förster's equation was only possible in the case where each chromophore possesses a definite direction of the transition moment. Comparison of the simulated decay profiles of $r(t)$ (Figure 10b,c) with the experimentally observed

(26) Berlman, I. B. *Energy Transfer Parameters of Aromatic Compounds*; Academic: New York, 1973.

(27) Perrin, D. D.; Armarego, W. L. F.; Perrin, D. R. *Purification of Laboratory Chemicals*; Pergamon: Oxford, 1980. The refractive index increases as temperature decreases. However, its temperature dependence is very small ($dn/dt = \sim -10^{-4}$ K^{-1}); therefore, it is reasonably assumed that the results are not affected significantly by the use of the n value at 20 °C.

(28) Computer programs (Fortran 77 and Basic) on the conformational analysis, the distribution functions, and the simulation process are available on request.

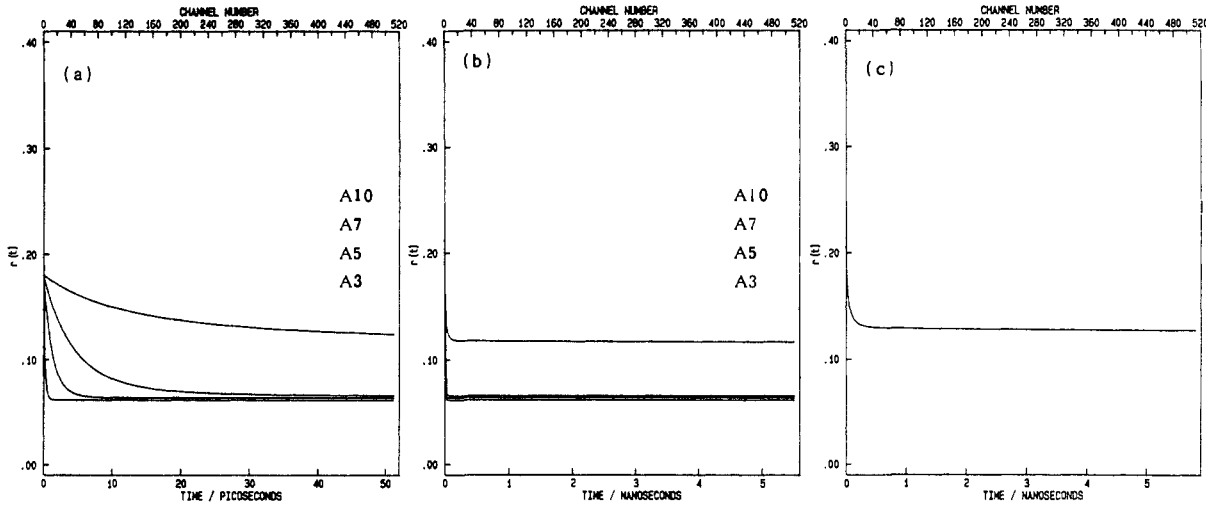

Figure 10. Expected decays of fluorescence anisotropy obtained by computer simulation based on the results of conformational analysis: (a) A3, A5, A7, and A10, time division 0.1 ps/channel, $r_0 = 0.18$; (b) A3, A5, A7, and A10, time division 10.73 ps/channel, $r_0 = 0.18$; (c) A12, time division 11.36 ps/channel, $r_0 = 0.206$.

decay profiles (Figure 4A,B) revealed that the experimentally observed decay profiles were well reproduced by the simulated decay curves.

In A3 and A5, the initial decays of $r(t)$ could not be observed (Figure 4) because of higher hopping rates than those detectable with our apparatus, and this behavior was exactly reflected in the simulated curves (Figure 10b). Furthermore, the experimentally observed values of the residual polarization, r_∞, were in good agreement with the simulated values of r_∞. In particular, in the experimentally observed curves, r_∞ increased in the order A3 < A5 < A7, although the differences were very small. This behavior was well reproduced in the simulated curves. In addition, in Figure 4A r_∞ of A10 was much larger than in A3, A5, and A7, which may be a consequence of the odd–even effect associated with alkyl spacers. In fact, the angular distributions of θ_S in A10 and A12 were clearly different from those of A3, A5, and A7, which exhibited similar distribution functions (Figure 9). The r_∞ values are predominantly determined by relative orientation of the two anthryl groups; thus, excellent agreement between the experimentally observed curves and the simulated ones demonstrates that the actual orientation of Am is well reflected in the potential energy calculation.

It must be mentioned here, however, that agreement of the residual polarization values of A3 and A5 with the simulated values of r_∞ does not imply validity of Förster's mechanism to these molecules. Applicability of Förster's mechanism to these molecules is judged only if the decay profiles are precisely analyzed, since the residual polarization is expected to depend only on the mutual orientation of the relevant chromophores and not on the mechanism of excitation hopping.

On the basis of eqs 8 and 13, the decay of $r(t)$ is essentially multiexponential with numerous components of ω_i and r_{1i}; thus, the decay analysis for $r(t)$ on the basis of the iterative nonlinear least-squares method provides no precise values of ω_i unless many components are considered. However, as one can see in Figures 7 and 9, the distributions of R and θ_S are rather narrow; thus, analysis of the experimentally observed decays of $r(t)$ with a singly exponential function (eq 14) may give a rough estimate for the

$$r(t) = A \exp(-2\omega t) + B \qquad (14)$$

experimentally obtained excitation hopping rates. Here, A, B, and ω are fitting parameters. In Table III, these parameters obtained by the fitting procedure are listed together with the values of reduced χ^2 and Durbin–Watson (DW) parameters used to judge the goodness of the fittings. The hopping rate constants observed for Am are larger by approximately 2 orders of magnitude than those observed for α,ω-bis(2-naphthyl)-n-alkanes[15] when compared between the compounds with the same alkyl spacer length. This is mainly attributable to larger values of ϕ_D and ϵ_A and shorter τ_D of the anthryl moiety than those of the 2-naphthyl moiety. From the lifetimes and the hopping rate constants, we can estimate the hopping frequency during the lifetime, which are listed in the last column of Table III. In A7, the hopping frequency is ~28 and this value is ~18 times larger than that of α,ω-(2-naphthyl)heptane.[15]

Table III. Excitation Hopping Parameters Obtained by the Best Fit Curves[a]

	A	B	ω, s^{-1}	χ^2	DW	freq
A3						
A5						
A7	0.081	0.072	2.5×10^9	0.7872	2.0789	28
A10	0.120	0.110	1.6×10^9	0.7211	1.9687	18
A12	0.194	0.135	1.1×10^9	0.6899	1.8404	12
A14	0.204	0.158	6.8×10^8	0.7455	1.8250	7.5
A18	0.185	0.149	6.4×10^8	0.8345	1.9795	7

[a] Obtained by fitting of the experimentally observed curves of $r(t)$ with eq 14, $r(t) = A \exp(-2\omega t) + B$.